A model with a unified kinematic hardening law for cyclic behavior of stiff clays

P. Y. Hong[a], J. M. Pereira[a,*], Y. J. Cui[a], A. M. Tang[a], F. Collin[b], X.L. Li[c]

[a]*Université Paris-Est, Laboratoire Navier (UMR 8205), CNRS, ENPC, IFSTTAR, F-77455 Marne-la-Vallée, France*

[b]*Department GeomaC, University of Liège, Sart Tilman B52/3, Chemin des Chevreuils, 1, B-4000, Liege, Belgium*

[c]*European Underground Research Infrastructure for Disposal of Nuclear Waste in Clay Environment, ESV EURIDICE GIE, Mol, Belgium.*

Abstract: This paper presents a kinematic hardening model for describing some important features of natural stiff clays under cyclic loading conditions, such as closed hysteretic loops, smooth transition from the elastic behavior to the elastoplastic one and changes of the compression slope with loading/unloading loops. The model includes two yield surfaces, an inner surface and a bounding surface. A non-associated flow rule and a unified kinematic hardening law are proposed for the inner surface. The adopted hardening law enables the plastic modulus to vary smoothly when the kinematic yield surface approaches the bounding surface and ensures at the same time the non-intersection of the two yield surfaces. Furthermore, the first loading, unloading, and reloading stages are treated differently by applying distinct hardening parameters. The main feature of the model is that its constitutive equations can be simply formulated based on the consistency condition for the inner yield surface based on the proposed unified kinematic hardening law; thereby, this model can be easily implemented in a finite element code using a classic stress integration scheme as for the modified Cam Clay model. The simulation results on the Boom Clay, natural stiff clay, have revealed the relevance of the model: a good agreement has been obtained between simulations and the experimental results from the tests with different stress paths under cyclic loading conditions. In particular, the model can satisfactorily describe the complex case of oedometric conditions where the deviator stress is positive upon loading (compression) but can become negative upon unloading (extension).

Keywords: natural stiff clay; kinematic hardening; cyclic loading; elastoplasticity; stress integration; validation

*Correspondance to: École des Ponts ParisTech, Laboratoire Navier–CERMES, 6-8 av. B. Pascal, 77455 Marne-la-Vallée cedex 2, France

Email address: jeanmichel.pereira@enpc.fr (J. M. Pereira)

Preprint submitted to Computers and Geotechnics

1. Introduction

It is well known that the stress-strain curves of soils under cyclic loading conditions show hysteresis loops with gradual accumulation of permanent strain. Indeed, various experimental results from isotropic compression tests, drained triaixal shear tests and oedometer tests on natural stiff clays (Boom Clay and Ypresian Clays, for instance) with several unloading/reloading cycles show marked hysteresis loops [1, 2, 3]. Natural stiff clays also exhibit smooth transition from elastic to elastoplastic compression (progressive stiffness degradation with strain) for either loading or unloading/reloading stages. In addition, experiments show another important characteristic regarding the compression slope in the reloading process before reaching σ'_{vmax} which is the maximum vertical stress applied before unloading. This compression slope in the reloading process varies significantly from one loop to another. Nguyen [4] concluded that this slope increases with σ'_{vmax}. These features must be taken into account when developing constitutive models for the description of the mechanical behavior of this kind of clays under cyclic loading conditions.

Conventional critical state models for soils including the Modified Cam Clay model (MCC) can describe plastic strains in the normally consolidated state, but only elastic strains is produced during the subsequent unloading–reloading cycles within the yield surface. On the other hand, bounding surface models with radial mapping rule proposed in the 1980s (see e.g. [5, 6]), where the current plastic modulus varies with the distance between the stress state and its image point on the bounding surface, can successfully describe some important features of natural stiff clays such as the smooth transition from elastic to elastoplastic states as well as the softening behavior. However, this kind of the models gives open hysteresis loops during unloading-reloading stages and cannot describe the cyclic loading behavior realistically, since no plastic strain is generated during the unloading process. To overcome this deficiency, attempts were made by some researchers (e.g. [7, 8]]) by applying the generalized plasticity concept proposed by Zienkiewicz and Mroz [9]. It is assumed that plastic strain is produced even by a stress increment directed toward the inside of the yield surface, the stress point always lying on the inner yield surface. With the generalized plasticity concept, a gradual strain accumulation with closed hysteresis loops can be simulated for the loading compression side (the deviator stress is positive). However, it fails for the extension side (negative deviator stress): an inflection appears in the stress-strain curve upon unloading along a straight stress path [10] as illustrated in Fig. 1. It is assumed that the loading yield surface has

an ellipse shape as in the MCC model (see Fig. 1 (a)). During the unloading process (path 1-2), the loading surface shrinks from f_{l1} to f_{l2} with the size parameter decrease from p'_{c1} to p'_{c2}. A negative plastic strain increment is generated for this loading path. When point 3 is reached, the direction of the effective stress rate becomes tangential to the loading surface and just elastic strain is produced leading to an inflection point (see Fig. 1 (b)). After point 3, the loading surface expands along p' axis passing through the origin of the stress space with a positive plastic strain increment generated. Indeed, the predicted behavior that a negative plastic strain increment generated along path 1-3 but a positive plastic strain increment along path 3-4 is difficult to admit physically. Hence, this kind of the models is not suitable for simulating the oedometer tests where negative deviator stress occurs in the unloading process.

Commentaire [JMP1]: No

I do not understand your comments.

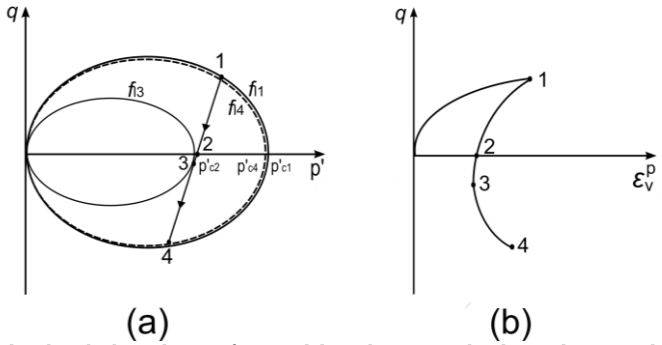

Fig. 1. Problems related to the bounding surface models with isotropic hardening law considering plastic strain in the unloading process: (a) the stress path in the (p', q) plane and (b) the stress-volumetric plastic strain curve

An important development in the constitutive modeling for the cyclic loading behavior is the introduction of kinematic hardening mechanism by Mroz (1967) [11]. The 'Bubble' model by Al-Tabbaa (1989) [12] was developed within the framework of kinematic models. In this model, a kinematic yield surface (namely bubble surface) is defined, which is allowed to translate and expand or contract within the conventional yield surface (namely bounding surface). The formulation of such a kinematic hardening model is mainly centered on the translation rule and the hardening function: the former is used to control the movement and interaction of the two surfaces and the latter is defined to describe the variation of the plastic modulus. This model can reproduce a closed hysteretic loop under a complete cyclic loading with deviator stress being from positive values to negative values. However, it should be pointed out that in the bubble model, the plastic modulus of the current stress state is not formulated by considering the consistency condition of the kinematic yield surface, but given by an interpolation function depending on the distance from the current stress point to the

bounding surface. In addition, the kinematic hardening models are still not widely used to describe the cyclic behavior of natural stiff clays, such as Boom Clay.

In this study, a kinematic hardening model for modeling the cyclic behavior of natural stiff clays is developed. Basically, the developed model has a structure similar to that of bubble models. However, instead of defining an interpolation function for the plastic hardening modulus, a unified kinematic hardening law associated with the kinematic yield surface is defined, enabling the plastic modulus to vary smoothly along a plastic loading process. With a translation rule incorporated, this hardening law ensures that the two yield surfaces do not intersect but tend to coincide at the current stress point. Thereby, the constitutive equations can be simply obtained based on the consistency condition of the kinematic yield surface which is equivalent to the classic yield surface. Hence, in the numerical implementation, all the features of the stress integration schemes for classic elastoplastic models can be applied. This allows the model to be employed easily in the analysis of geotechnical problems. Furthermore, different model parameters for describing hardening rate in the loading/unloading/reloading processes are introduced enabling the cyclic loading behavior of natural stiff clays to be described in a flexible fashion. Also, a non-associated flow rule is adopted in order to properly describe the dilatancy behavior. The simulation of a series of tests on natural Boom Clay along different loading paths including the complex oedometric path show the relevance of the model proposed.

2. Model description

For the sake of simplicity, it is assumed that the soil behavior is isotropic. This hypothesis will clearly limit the proposed constitutive model if inherent and induced anisotropy is to be described. However, the extension of this model to an anisotropic elasto-plastic model is feasible by incorporating new plastic mechanisms such as a rotational hardening rule associated with an inclined surface as proposed by Wheeler *et al.* [13].

In what follows, the constitutive model is developed and formulated in the conventional triaxial conditions, i.e., when two effective principal effective stresses are equal ($\sigma'_2 = \sigma'_3$). The model can be extended to a general stress state easily if the soil parameters are properly determined as pointed out by Morz *et al.* [14]. By defining the compressive stresses and strains as positive, the mean effective stress $p' = p - u$ with u as the pore water pressure and the deviator stress q are defined as follows:

$$p' = \frac{1}{3}\left(\sigma'_1 + 2\sigma'_3\right) \qquad q = \sigma'_1 - \sigma'_3 \tag{1}$$

where σ'_1 and σ'_3 are the axial and lateral effective stresses, respectively.

The volumetric strain ε_v and the shear strain ε_s are defined as:

$$\varepsilon_v = \varepsilon_1 + 2\varepsilon_3 \qquad \varepsilon_s = \varepsilon_1 - \varepsilon_3 \tag{2}$$

where ε_1 and ε_3 are the axial and lateral strains, respectively.

2.1. Elastic behavior

As in the MCC, the elastic volumetric strain increment is given by:

$$d\varepsilon_v^e = \frac{dp'}{K} \tag{3}$$

with the elastic bulk modulus as follows:

$$K = \frac{v_0 p'}{\kappa} \tag{4}$$

where κ is the elastic slope in a specific volume-logarithmic mean stress plane (v, ln p') and v_0 is the initial specific volume.

The elastic shear strain increment can be calculated by:

$$d\varepsilon_s^e = \frac{dq}{3G} \tag{5}$$

and the shear modulus G can be calculated with a constant Poisson's ratio ν:

$$G = \frac{3(1-2\nu)K}{2(1+\nu)} \tag{6}$$

It is well-known that this choice for shear modulus (Eq (6)) helps in simulating experimental results, but leads to thermodynamic inconsistency since the Maxwell symmetry relations are not satisfied in this case [15, 16].

2.2 Plastic behavior

2.2.1 Yield surfaces

Two yield surfaces are introduced (see Fig. 2): an outer yield surface namely bounding surface (f_b) that represents the normal consolidation behavior and an inner kinematic yield surface (f_k) that delimits an elastic domain. The yield behavior is described in terms of evolutions of the kinematic yield surface within the domain delimited by the bounding surface.

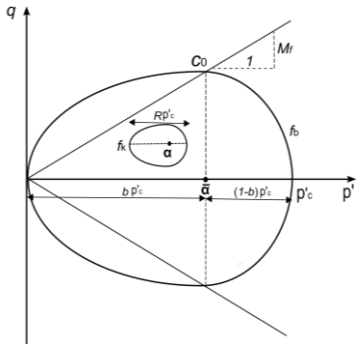

Fig. 2. Kinematic hardening model: Bounding surface and kinematic yield surface

To achieve a wide variety of yield surface shapes, a smooth 'egg-shape' yield surface inspired from Eekelen *et al.* [17] is used for the bounding surface (f_b). The yield locus f_b as seen in Fig. 2 consists of two ellipses having the same center $\bar{\boldsymbol{\alpha}}\left(\bar{\alpha}_p,\bar{\alpha}_q\right)$ but different horizontal axis lengths, bp'_c for the left part and $(1\text{-}b)p'_c$ for the right part. At the apex of the two ellipses (see point C_0) where they touch each other, the tangent to both ellipses is horizontal. The slope of the diagonal of the left ellipse is M_f, the same as in the MCC model. Thus, the yield function is defined as follows:

$$\begin{aligned} f &\equiv \left(p'-\bar{\alpha}_p\right)^2+\frac{\left(q-\bar{\alpha}_q\right)^2}{M_f{}^2}-p_c'^2=0 \qquad \left(for \quad p'\le\bar{\alpha}_p\right) \\ f &\equiv \left(p'-\bar{\alpha}_p\right)^2+\frac{(1-b)^2\left(q-\bar{\alpha}_q\right)^2}{b^2M_f{}^2}-p_c'^2=0 \qquad \left(for \quad p'>\bar{\alpha}_p\right) \end{aligned} \tag{7}$$

Commentaire [JMP2]: Some p' missing
I correct all the equations.

where p'_c is the conventional preconsolidation pressure defining the size of the bounding surface and b is a material parameter. Since the bounding surface passes through the origin in (p', q) plane and develops along the hydrostatic axis, $\bar{\alpha}_p = bp'_c$ and $\bar{\alpha}_q = 0$ will always hold in the yield surface evolution. It is worth noting that the MCC model is obtained when b = 1/2.

It is assumed that the inner kinematic yield surface has a similar shape but a size R ($0 < R < 1$) times that of the bounding surface. Thus, the equations of the kinematic surface (f_k) take the following form:

$$f \equiv \left(p' - \alpha_p\right)^2 + \frac{\left(q - \alpha_q\right)^2}{M_f^{\,2}} - \left(Rp'_c\right)^2 = 0 \qquad \left(for \quad p' \le \alpha_p\right)$$
$$f \equiv \left(p' - \alpha_p\right)^2 + \frac{(1-b)^2\left(q - \alpha_q\right)^2}{b^2 M_f^{\,2}} - \left(Rp'_c\right)^2 = 0 \qquad \left(for \quad p' > \alpha_p\right) \tag{8}$$

where $\boldsymbol{\alpha}(\alpha_p, \alpha_q)$ is the coordinates that specify the position of the center of the kinematic yield surface.

2.2.2 Isotropic hardening law

The isotropic hardening law is defined to describe the evolution of the bounding surface size (through parameter p'_c) with plastic strains. The evolution of p'_c depends on the plastic volumetric strain ε_v^p as in the MCC model, and is given by:

$$dp'_c = \frac{v_0 p'_c}{\lambda - \kappa} d\varepsilon_v^p \tag{9}$$

where λ is the normal consolidation slope in $(v, \ln p')$ plane. This isotropic hardening law also applies implicitly to the kinematic yield surface through the constant ratio R as the kinematic yield surface is activated.

2.2.3 Kinematic hardening law

Consider now the kinematic hardening law for the kinematic yield surface. The current stress state is defined as $\boldsymbol{\sigma}' = \{p', q\}^T$ (point A in Fig. 3) which lies on the kinematic surface is associated with a conjugated stress state $\bar{\boldsymbol{\sigma}}' = \{\bar{p}', \bar{q}\}$ (point B in Fig. 3) on the bounding surface having the same direction of the exterior normal, as illustrated in Fig. 3. The similarity of the kinematic yield surface and the bounding surface gives the following relationship:

$$\left(\boldsymbol{\sigma}' - \boldsymbol{\alpha}\right) = R\left(\bar{\boldsymbol{\sigma}}' - \bar{\boldsymbol{\alpha}}\right) \tag{10}$$

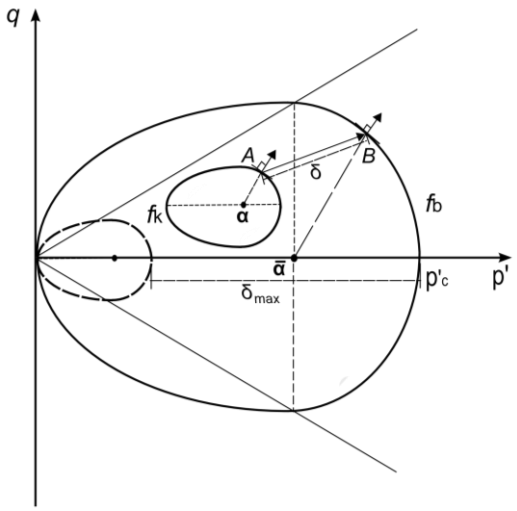

Fig. 3. Schematic representation of the kinematic hardening law

To account for the progressive increment of plastic strain as the kinematic yield surface approaches the bounding surface, a scalar *r* measuring the normalized distance of the current stress state on the kinematic yield surface to the associated conjugated stress state on the bounding surface is defined as follows:

$$r = \frac{\delta}{\delta_{max}} \tag{11}$$

where $\delta = \left|\boldsymbol{\sigma}' - \bar{\boldsymbol{\sigma}}'\right|$ is the current distance between the current stress state and the conjugated stress state, δ_{max} denotes the maximum distance: $\delta_{max} = (1-R)\,p'_c$. Obviously, $r = 0$ holds when the two surfaces are in contact.

Commentaire [JMP3]: Add these distances to fig.2
I add them.

A simple law is defined to describe the evolution of *r* following Borja *et al.* [18]:

$$dr = -s\frac{v_0}{\lambda-\kappa} r^2 d\varepsilon_d^p \tag{12}$$

with a generalized plastic strain defined in Eq (13) to account for the contribution of both the volumetric and shear plastic strains:

$$d\varepsilon_d^p = \sqrt{\left(d\varepsilon_v^p\right)^2 + A_d\left(d\varepsilon_s^p\right)^2} \tag{13}$$

where s is a parameter describing the degradation of the stress–strain curve inside the bounding surface; A_d is a parameter which controls the contribution of shear plastic strain. Note that such a combined volumetric-deviatoric hardening law enables the stress increase over the critical state line along non-isotropic stress paths and thus enables the plastic dilatancy to be described.

The contribution of Eq (13) is illustrated in Fig. 4 through an isotropic loading-unloading path O_1CDEF. The initial effective stress state is represented by point O_1. For the stress path O_1C, only elastic strain occurs. Upon further loading, the bubble will be pulled along the stress path and in the meanwhile plastic strain is generated. Due to the plastic strain generation, the kinematic yield surface and the bubble model will expand (not shown in Fig. 4). The volumetric plastic strain produced along the stress path CD can be calculated from Eq (9) and Eq (12) :

$$\frac{dp'}{p'} = \frac{v_0}{\lambda - \kappa}\left[1 + s\left(1 + R\right)r\right]d\varepsilon_v^p \tag{14}$$

When parameter r decreases from its initial value r_0 to 0, the stress point moves toward the bounding surface and the overall hardening modulus decreases. This hardening law enables a smooth elastic-plastic transition. If r = 0, the two surfaces are in contact at point D and the contribution of Eq (12) vanishes. In that case, the isotropic hardening law applies, and any further loading process will move the two surfaces together. If the soil is now unloaded such that the stress path travels along stress path DE, the soil behaves elastically first with generation of expansive (negative) elastic strain. Along stress path EF, expansive plastic strain is produced. The volumetric plastic strain produced along stress path EF can also be calculated from Eq (9) and Eq (12):

$$\frac{dp'}{p'} = \frac{v_0}{\lambda - \kappa}\left[1 + s\left(1 + R\right)r\right]d\varepsilon_v^p \tag{15}$$

Like in the loading process, in the unloading process the hardening modulus decreases as the stress moves toward the inside of the bounding surface with r decreases from another initial value of r_0 to 0. A smooth elastic-plastic behavior in the unloading process can also be simulated.

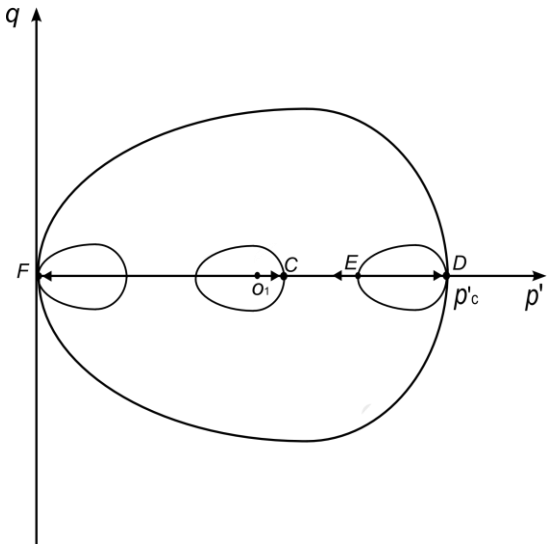

Fig. 4. Relative configuration of the kinematic yield surface and bubble surfaces

Note that it is not guaranteed that the kinematic yield surface do not intersect the bounding surface in the plastic loading process just with Eq (12). This can be remediated by defining a translation rule that guarantees that both surfaces ($f_k = 0$ and $f_b = 0$) do not intersect but are in contact at a point where they share the same normal. This can be done by assuming that the relative motion of point A with respect to B (see Fig. 3) is directed along vector ($\boldsymbol{\beta} = \bar{\boldsymbol{\sigma}}' - \boldsymbol{\sigma}'$) [14]. The following expression can then be obtained:

$$d\left(\boldsymbol{\sigma}' - \bar{\boldsymbol{\sigma}}'\right) = d\mu\left(\bar{\boldsymbol{\sigma}}' - \boldsymbol{\sigma}'\right) \tag{16}$$

where $d\mu$ is a scalar factor.

To define a unified hardening law, Eq (12) and Eq (16) should be made compatible. For this purpose, $d\mu$ is defined as:

$$d\mu = \frac{v_0}{\lambda - \kappa}\left(srd\varepsilon_d^p - d\varepsilon_v^p\right) \tag{17}$$

Eq (16) can now be rewritten by substituting Eq (9) and Eq (17) :

$$d\left[\frac{\left(\bar{\boldsymbol{\sigma}}' - \boldsymbol{\sigma}'\right)}{\delta_{max}}\right] = -s\frac{v_0}{\lambda - \kappa}\frac{\left(\bar{\boldsymbol{\sigma}}' - \boldsymbol{\sigma}'\right)}{\delta_{max}}rd\varepsilon_d^p \tag{18}$$

which satisfies Eq (12).

Commentaire [JMP4]: (9) is isotropic (p'c)
Yes, with Eq (9) depsilonvp in Eq (17) then can be replaced by a function of p'c and dp'c . Since P'c=\detamax/(1-R), Eq (16) can be rewritten with the form having \detamax .

Substituting the geometric relation given by Eq (10) into Eq (18) gives a unified kinematic hardening law:

$$d\boldsymbol{\alpha} = \frac{v_0}{\lambda - \kappa}\left(s r d\varepsilon_d^p - d\varepsilon_v^p\right)\left(\bar{\boldsymbol{\sigma}}' - \boldsymbol{\sigma}'\right) + \frac{(1-R)dp_c'}{Rp_c'}\left(\boldsymbol{\sigma}' - \boldsymbol{\alpha}\right) + d\bar{\boldsymbol{\alpha}} \qquad \textbf{(19)}$$

This kinematic hardening law specifies the translation of the centre of the kinematic yield surface and enables the plastic modulus to vary at the same time, having a unified function of the hardening law and the translation rule in a classic kinematic hardening model.

2.2.4 Hardening parameter s and loading cycles

To satisfactorily describe the closed hysteretic loop behavior, a well-known solution is to divide the whole cyclic loading process into three parts, namely first loading, unloading and reloading processes (e.g. [19, 20]). For each part, a specific expression of plastic modulus is used to control the corresponding slope of the stress-strain curve. Following this concept, parameters s_0, s_u and s_r are introduced to control the hardening rate for the first loading, unloading and reloading processes, respectively.

Furthermore, as mentioned before, an important behavior regarding slope C_{cp} in the reloading process before reaching σ'_{vmax} (the maximum vertical stress applied before unloading) has been observed experimentally: C_{cp} varies significantly from one loop to the next one. For Boom Clay and Ypresian Clays, oedometer tests have revealed that C_{cp} varies linearly with the logarithm of σ'_{vmax} [4]. Since K_0 (the coefficient of earth pressure at rest) is close to 1 for natural Boom Clay (K_0 = 0.80) and Ypresian Clays (K_0 = 0.88) [21, 22], the vertical effective stress state can then be approximated by the mean effective stress. Therefore, the following expression can be adopted for hardening parameter s_r :

$$s_r = s_0 + \lambda_s \, log\left(\frac{p_r'}{p_{max}'}\right) \qquad (20)$$

where λ_s is a material constant which controls the variation rate of s_r; p'_r is the initial mean effective stress in the reloading process; p'_{max} is the maximum mean effective stress applied before unloading. This equation ensures that the higher the value of p'_{max} or the lower the value of p'_r, the lower the value of s_r, thus the straighter the stress-strain curve for the reloading before reaching p'_{max} (or σ'_{vmax}).

2.2.5 Flow rule

Commentaire [JMP5]: Don't you have a problem with the sign of \sigma-\bar\sigma
I am sorry that I don't see the problem. This is the classic equation describing geometric similarities of the two surfaces. Could you please explain the problem in more detail?

Commentaire [JMP6]: Why do you call it unified. This is not clear
This kinematic hardening law, unlike in a classic kinematic hardening model, has a unified function of hardening law and translation rule. I want to highlight this characteristic. So I call it unified hardening law. Do you think it is necessary to name it? If it does, do you have an appropriate word?

In the common critical state models, the phenomenological interaction between shear and volume change (contraction and dilatancy) has been well handled by specifying an appropriate flow rule. In the well-known MCC model, the flow rule is defined as follows:

$$\frac{d\varepsilon_v^p}{d\varepsilon_s^p} = \frac{M_g{}^2 - \eta^2}{2\eta} \tag{21}$$

where η is the stress ratio q/p'; M_g is the critical state slope corresponding to the stress ratio when there is no further volumetric strain. In the loading process, if $\eta < M_g$, plastic compression occurs; if $\eta > M_g$, plastic dilatancy occurs.

If an associated plastic flow rule is adopted in this model, it gives

$$\begin{aligned} \frac{d\varepsilon_v^p}{d\varepsilon_s^p} &= \frac{\left(p' - \alpha_p\right) M_f{}^2}{q - \alpha_q} \qquad \left(for \quad p' \le \alpha_p\right) \\ \frac{d\varepsilon_v^p}{d\varepsilon_s^p} &= \frac{\left(p' - \alpha_p\right) b^2 M_f{}^2}{\left(1-b\right)^2 \left(q - \alpha_q\right)} \qquad \left(for \quad p' > \alpha_p\right) \end{aligned} \tag{22}$$

where $M_f = M_g$ holds in the associated flow rule.

It can be clearly seen that the contractive plastic phase, dilative phase and the critical state controlled by Eq (22) depends on the relative position between the current effective stress state and the center of kinematic yield surface, instead of the value of $M_g - \eta$ as in the MCC model. Hence, a non-associated flow rule is defined by modifying the associated flow rule expressed by Eq (22) :

Commentaire [JMP7]: Unclear
I rewrite this part.

$$\begin{aligned} \frac{d\varepsilon_v^p}{d\varepsilon_s^p} &= \frac{\left(M_g - \eta\right)\left(2p' - 2\alpha_p + Rp_c'\right)}{k_g\left[2\left(q - \alpha_q\right) + Rp_c'\right]} \qquad \textbf{when loading/reloading} \\ \frac{d\varepsilon_v^p}{d\varepsilon_s^p} &= \frac{\left(M_g + \eta\right)\left(2p' - 2\alpha_p - Rp_c'\right)}{k_g\left[2\left(q - \alpha_q\right) - Rp_c'\right]} \qquad \textbf{when unloading} \end{aligned} \tag{23}$$

where k_g is a material constant that is used to control the magnitude of the ratio of plastic volumetric strain increment to plastic shear strain increment. During loading, the sign of Eq (23) is controlled by the value of $M_g - \eta$. This value allows distinguishing the plastic contractive phase, plastic dilative phase and the critical state. Similarly, during unloading, Eq (23) defines the plastic contractive phase, the plastic dilative phase, and the critical state when $\eta > -M_g$, $\eta < -M_g$ and $\eta = -M_g$, respectively.

2.5 Constitutive equations

In the following, the equations for the plastic strain increment are formulated by considering the consistency condition for the kinematic yield surface. The formulations are given in triaxial {p', q} space. The stress and strain variables write as follows:

$$\boldsymbol{\sigma}' = \{p', q\}^T, \quad \boldsymbol{\varepsilon} = \{\varepsilon_v, \varepsilon_s\}^T \tag{24}$$

The plastic strain increment is computed from the plastic potential as follows:

$$d\boldsymbol{\varepsilon}^p = d\lambda \frac{\partial g}{\partial \boldsymbol{\sigma}'} \tag{25}$$

Commentaire [JMP8]: Be careful: you mix triaxial stress space and tensor form while \sigma is also used for the translation rule and has another meaning
Yes, I mixed them. To simply solve this problem, I re-defined the stress strain variable (\sigma and \epsilon) and give the constitutive equations in triaxial space.

where $d\lambda$ is a positive scalar namely plastic multiplier; g is the plastic potential.

$\boldsymbol{\alpha}$ and p'_c act as hardening variables. Therefore, the consistency condition of the kinematic yield surface is given by:

$$\left(\frac{\partial f_k}{\partial \boldsymbol{\sigma}'}\right)^T : d\boldsymbol{\sigma}' + \left(\frac{\partial f_k}{\partial \boldsymbol{\alpha}}\right)^T : d\boldsymbol{\alpha} + \frac{\partial f_k}{\partial p'_c} dp'_c = 0 \tag{26}$$

Substituting Eqs (9), (19) and (25) into Eq (26) gives:

$$\left(\frac{\partial f_k}{\partial \boldsymbol{\sigma}'}\right)^t : d\boldsymbol{\sigma}' - h d\lambda = 0 \tag{27}$$

with h being the hardening modulus:

$$h = -\left(\frac{\partial f_k}{\partial \boldsymbol{\alpha}}\right)^T \frac{v_0}{\lambda - \kappa}\left[\left(sr\sqrt{\frac{\partial g}{\partial p'}^2 + A_d \frac{\partial g}{\partial q}^2} - \frac{\partial g}{\partial p'}\right)\left(\bar{\boldsymbol{\sigma}}' - \boldsymbol{\sigma}'\right) + \frac{(1-R)}{R}\frac{\partial g}{\partial p'}\left(\boldsymbol{\sigma}' - \boldsymbol{\alpha}\right) + bp'_c \frac{\partial g}{\partial p'}\right] - \frac{\partial f}{\partial p'_c}\frac{v_0 p'_c}{\lambda - \kappa}\frac{\partial g}{\partial p'} \tag{28}$$

Commentaire [JMP9]:
- ‘ missing
- p’_c instead of p’_0
- f_k instead of f

I correct them.

From Eq (28), we can see that even when the stress state reaches the condition $\eta = M_g$, the inclusion of the shear hardening part ($\frac{\partial g}{\partial q} > 0$) leads to $h > 0$. With further loading, the effective stress increases over the critical state line and negative plastic volumetric strain occurs.

The stress-strain equations can finally be obtained in a differential form:

$$d\boldsymbol{\sigma}' = \mathbf{D}^{ep} d\boldsymbol{\varepsilon} \tag{29}$$

where:

$$\mathbf{D}^{ep} = \mathbf{D}^{e} - \mathbf{D}^{e} \frac{\mathbf{b}\left(\mathbf{a}\right)^{T} \mathbf{D}^{e}}{\left(\mathbf{a}\right)^{T} \mathbf{D}^{e}\mathbf{b} + h} \tag{30}$$

and $\mathbf{D}^{e}$ is the elastic stiffness matrix, $\mathbf{a} = \frac{\partial f_k}{\partial \boldsymbol{\sigma}'}$, $\mathbf{b} = \frac{\partial g}{\partial \boldsymbol{\sigma}'}$.

3. Determination of parameters

The proposed kinematic hardening model has 13 parameters (λ, κ, p'_{c0}, v, M_g, R, M_f, b, k_g, s_0, s_u, λ_s, A_d). The procedure for determining these parameters is described as follows.

1. λ, κ, p'_{c0}, v, M_g are common parameters in the MCC model. λ is the slope of the normal consolidation compression line and κ is the slope of swelling line of the isotropic compression curve in (v, ln p') plane. Note that κ is the parameter governing the elastic behavior. However, the proposed kinematic model assumes a purely elastic behavior only inside the kinematic yield surface in the initial stage of the loading/unloading/reloading processes. To be consistent with this elasto-plastic framework, κ can be determined by the swelling curve in the early stage of the unloading process. p'_{c0} denotes conventional isotropic preconsolidation pressure and it defines the initial size of the bounding surface. These three parameters (λ, κ and p'_{c0}) can be determined based on the isotropic compression curve in the (v, ln p') plane. The Poisson's ratio v can be determined from a standard triaxial test by considering the elastic behavior at a low strain level (around 0.5%) in the (ε_v, ε_1) plane: $\nu = \left(\varepsilon_v - \varepsilon_1\right)/2$. M_g is the critical state stress ratio which can be determined by the effective stress ratio at critical state.

2. R is the ratio of sizes of kinematic yield surface and bounding surface. The size of the kinematic yield surface is defined by R. Considering its physical meaning, this size can be determined in the early loading/unloading stage of isotropic compression test, based on the compression curve in the (v-ln p') plane.

3. M_f and b are parameters specifying the shape of the yield surface and can be calibrated by fitting the bounding yield surface shape to the conventional yield points obtained from the tests of different stress paths.

4. k_g is used in the plastic flow rule and can be determined by the values of $d\varepsilon_v^p / d\varepsilon_s^p$ obtained from drained triaxial shear tests.

5. Parameters s_0 and s_u determine the hardening rate for the first loading and unloading, respectively. λ_s is a material constant which controls the variation of the hardening rate in the reloading process. These three parameters can be back calibrated from an isotropic compression or oedometer test with at least two full unloading/reloading cycles.

4. Prediction and validation

In this section, the performance of the proposed model is assessed by simulating different tests on natural Boom Clay. This clay was taken in the Underground Research Laboratory (URL) at Mol, at a depth of 223 m. At this depth, the total vertical stress is around 4.5 MPa and the pore pressure is equal to 2.2 MPa, defining an effective vertical stress around 2.3 MPa [23]. As mentioned before, the value of K_0 being about 0.8, the initial effective stress state can be approximated by an isotropic one. As indicated by some researchers ([1, 24, 25]), saturating samples under low effective stresses induce significant swelling and the subsequent mechanical tests may not be representative of the behavior of natural Boom clay in field conditions. Therefore, only data obtained from the tests on samples saturated under the in-situ effective stress are considered in this study. The results that are taken into account include those from isotropic compression tests, drained triaixal shear tests and oedometer tests, carried out in different laboratories.

All the simulations are performed from a common point (p'_0 = 2 MPa, e_0 = 0.61) which is assumed to be on the initial kinematic yield surface. Parameters λ, κ and p'_{c0} were determined from the isotropic compression tests; k_g, A_d and v were calibrated using the experimental curves ε_v-ε_1 from two drained triaxial shear tests; M_f, k_f, b and M_g were derived from the conventional yield stresses and the critical stress ratio of all the drained triaxial shear tests; s_0, s_u and λ_s were calibrated from the oedometer test results. These parameters are presented in Table 1.

Table 1 Model parameters for natural Boom Clay

λ	κ	v	p'_{c0} (MPa)	R	M_f	b
0.18	0.02	0.3	6	0.15	0.7	0.65
M_g	k_g	s_0	s_u	λ_s	A_d	
0.67	0.14	40	14	10.3	0.2	

4.1 Isotropic compression test

Many isotropic compression tests on natural Boom Clay samples have been performed and some of them are summarized in Table 2 [1, 4, 26].

Table 2 Summary of the isotropic tests reported in literature

Test	Reference	Sample depth (m)	Initial void ratio	Void ratio after saturation
Iso-1	Baldi *et al.* [1]	223	0.677	-
Iso-2	Le [26]		0.620	0.590
Iso-3	Nguyen [4]		-	0.600

After completion of the saturation process, isotropic compression was performed under drained conditions: in Iso-1, the sample was loaded isotropically up to a mean effective stress of 4 MPa and then unloaded to 2 MPa, reloaded to 8 MPa, unloaded again to 2 MPa, and reloaded again to 5 MPa; in test Iso-2, the sample was loaded isotropically up to a mean effective stress of 10 MPa and then unloaded to 2 MPa; in test Iso-3, the sample was loaded isotropically up to 20 MPa and then unloaded to 0.5 MPa. The volumetric strains were obtained from the volume of drained-out water in all the three tests.

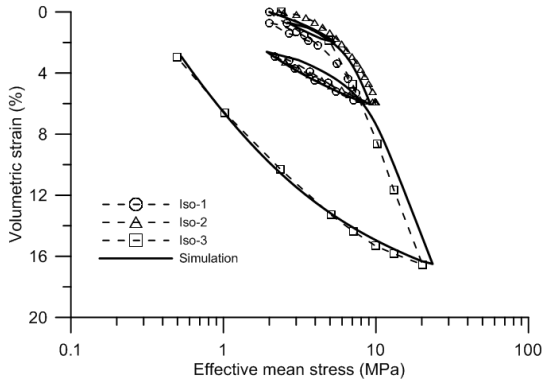

Fig. 5. Numerical simulations of isotropic compression cyclic tests.

Fig. 5 compares the model simulation and the experimental results. Note that the experimental data along the same loading path from different samples present a little scatter and the simulation cannot satisfy all the experimental data. Keeping this in mind, it can be observed that the model can capture the general trend of the experimental data in the loading-unloading-reloading processes and the difference between them is small. In particular, the hysteresis loops are simulated satisfactorily. Furthermore, the model can capture the smooth elasto-plastic behavior in each process of loading/unloading/reloading.

4.2 Triaxial shear test

The drained triaxial tests under cyclic loadings performed by Baldi *et al.* [1] are summarized in Table 3. These three tests CD-1 and CD-2 and CD-3 are performed under strain-controlled conditions. Strain reversals were applied at 0.60% and 2.80% of axial strains for CD-1 (Fig. 6), at 0.56% and 2.93% of axial strains for CD-2 (Fig.7), at 0.60% and 3.80% of axial strains for CD-3 (Fig.8), respectively.

Table 3 Summary of the drained triaxial tests reported in literature.

Test	Sample depth (m)	Water content (%)	Mean effective stress before shearing (MPa)	Initial void ratio	Shear rate (μm/min)
CD-1	223	25.8	2	0.705	1
CD-2		25.8	3	0.717	
CD-3		25.7	4	0.712	

Figs. 6-8 present a comparison between the experimental results and those predicted by the model for the drained triaxial tests. The results are presented in terms of variations of deviator stress and volumetric strain versus axial strain.

For test CD-1, the model predicts smooth responses as observed experimentally (Fig. 6). Furthermore, the volumetric dilatancy is predicted on the volumetric strain-axial strain curve at large axial strain levels (after 5%). This is because a non-associated flow rule is adopted allowing the stress state to be above the line $q = M_g p'$. For the unloading-reloading process, the model can predict the closed hysteresis loops, the first loop at a small strain level (ε_1 = 0.6%) and the second loop at a large strain level (ε_1 = 2.8%). The second predicted hysteresis loop is wider than the first one, in agreement with the experimental results.

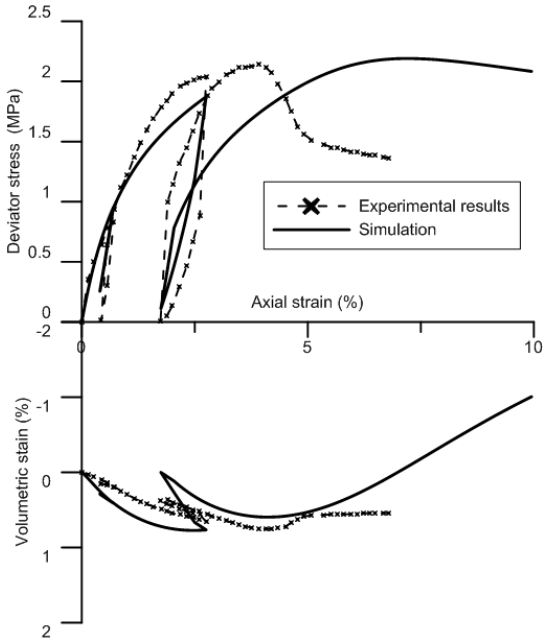

Fig. 6. Numerical simulations of drained triaxial shear cyclic test CD-1 (p'_0 = 2.0 MPa).

For test CD-2, the predictions agree well with the experimental data with a smooth elasto-plastic transition behavior on the deviator stress-axial strain curve as shown in Fig. 7. Though the volumetric strain given by the model is larger than the experimental one, the general trend is consistent. Again, the model can satisfactorily describe the hysteresis loops.

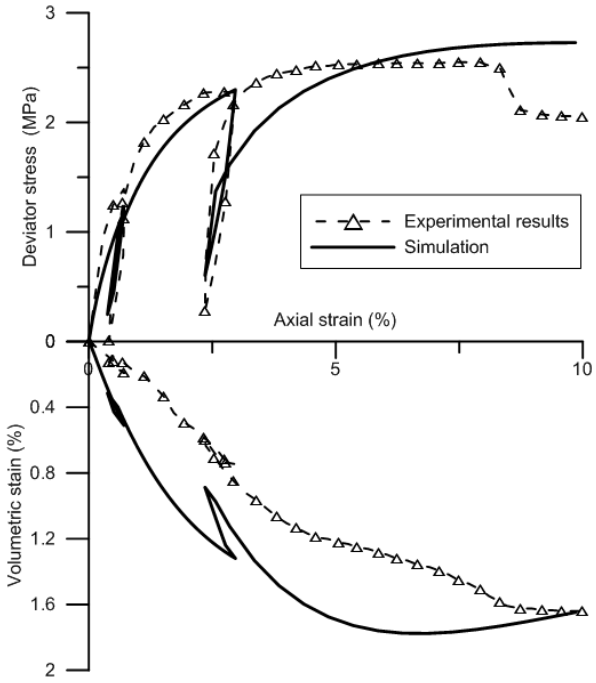

Fig. 7. Numerical simulations of drained triaxial shear cyclic test CD-2 (p'_0 = 3.0 MPa).

For test CD-3, it appears that the predictions agree well with the experimental results for the deviator stress-axial strain relationship even though a smaller hysteresis loop is predicted (Fig. 8). For the volume change, only contraction is predicted, in agreement with the test data.

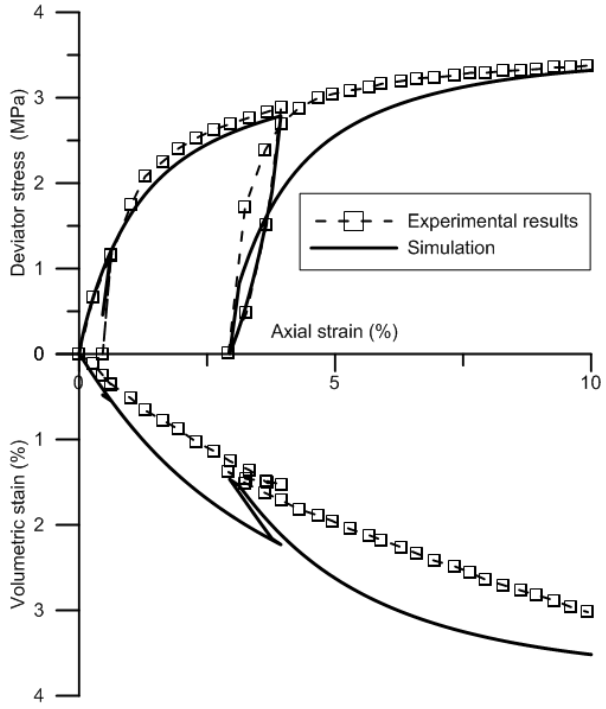

Fig. 8. Numerical simulations of drained triaxial shear cyclic test CD-3 (p'_0 = 4.0 MPa).

4.3 Oedometer tests

The oedometer tests conditions reported in literature are summarized in Table 4 [1, 3, 27].

Table 4 Summary of the odometer tests reported in literature.

Test	Reference	Sample depth (m)	Initial void ratio	Void ratio after saturation
Oed-1	Horseman *et al.* [3]	247	-	0.608
Oed-2	Deng *et al.* [27]	223	0.610	0.580
Oed-3	Baldi *et al.* [1]		0.696-0.717	-

In Oed-1 and Oed-2, the samples were saturated under a vertical effective stress of 1 MPa and no obvious swelling was found in the saturation process. Compression cycles were then applied, under the vertical effective stresses of 2, 8, 1, 32 and 1 MPa in Oed-1 and of 2, 16, 0.2, 32, and 0.1 MPa in Oed-2. In Oed-3, the sample was saturated under a higher vertical effective stress of 2.3 MPa. It was then loaded under 2 and 10 MPa effective vertical stresses.

Fig. 9 shows the comparison between the model predictions and the experimental data. It can be observed clearly that the simulation curves agree well with the experimental ones for each part of the loading paths, indicating the performance of the model in simulating smooth stress-

strain behavior. The important behavior of hysteresis loops under the cyclic loading paths is also well predicted. It is worth noting that during the unloading path in the second unloading-reloading loop, the stress path leads to negative values of deviator stress. The good correspondence between the model prediction and experimental data clearly shows the capability of the model in describing the behavior of soil under extension conditions. In the following reloading process, the predicted behavior is first purely elastic since the effective stress state moves inside the kinematic yield surface and then elasto-plastic after the stress path reaches the kinematic yield surface again.

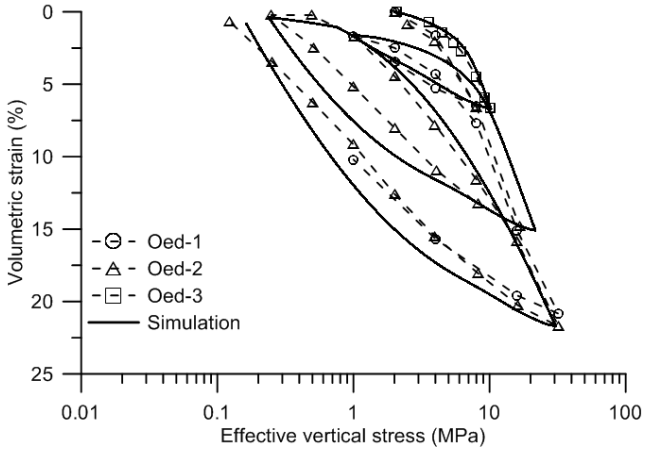

Fig. 9. Simulations of the oedometer tests.

From the experimental results from oedometer tests on natural stiff clays, Cui *et al.* [2] identified a mechanism involving the competition between the mechanical and physicochemical effects occurring during unloading or reloading. A threshold stress σ'_{vs} related to this mechanism was identified that separates the domain of large volume changes from the domain of small volume changes. Further analysis showed that this threshold stress corresponds physically to the swelling pressure of soil. It was observed that σ'_{vs} is function of the void ratio (e_i) just before the unloading or reloading process [4]:

$$\sigma'_{vs} = \gamma \exp(\beta e_i) \tag{31}$$

Commentaire [JMP10]: prefer exp() instead of e^()
I change it.

where γ and β are soil constants.

For Boom Clay, the values of γ = 231.4MPa and β = -8.0 are determined from the test data. The vertical swelling pressure σ'_{vs} calculated using Eq (31) is presented in Table 5 for each unloading/reloading process. On the other hand, using the proposed model, it is also possible to define a threshold stress (σ'_k) at each stage of unloading/reloading process based on the

initial kinematic yield surface, which divides the soil behavior into two parts: a part of purely elastic behavior with small volume changes and a part of elasto-plastic behavior with larger volume changes. Basically, σ'_{vs} and σ'_{k} have the same physical meaning. Thus, it is rational to make a comparison between them. For this purpose, the threshold stress σ'_{k} is determined using the proposed model and the obtained values are also presented in Table 5. Comparison between σ'_{vs} and σ'_{k} shows that the threshold stresses predicted by Eq (31) and the kinematic hardening model have the same general trend with the loading loops, but some difference exists, for instance, σ'_{k} =7.1 MPa and σ'_{vs} = 4.2 MPa for the first unloading process. This may be attributed to the experimental data scatter. Indeed, as observed before, the compression curves predicted by the model are in good agreement with the experimental ones for Oed-3, but there is some difference between the model and experiment in the case of Oed-1 and Oed-2 during the first loading process. As a result, a higher value of σ'_{k} is predicted in the following unloading path in comparison with σ'_{vs} based on the test data of Oed-1 and Oed-2.

Commentaire [JMP11]: and if you use Oed-3 to calculate sigma_vs?

In Oed-3, just a loading process is included without unloading/reloading process. So it is impossible to determine sigma_vs from its experimental results. However, the simulation for the loading part is closer to Oed-3 and then predicts a larger value of sigma_vs in comparison with the ones evaluated from experimental tests of Oed-1 and Oed-2.

Table 5 Predictions of the threshold stress in the loading/unloading/reloading loops

Loading phase	e_i	σ'_{vs} (MPa)	σ'_{k} (MPa)
1st unloading	0.503	4.2	7.1
1st reloading	0.583	2.1	1.6
2nd unloading	0.372	12.0	16.2
2nd reloading	0.606	1.8	0.9
3rd unloading	0.272	26.2	24.2

Summarizing, the developed model provides good predictions of the results from conventional experimental tests on natural Boom Clay. The smooth elasto-plastic behavior can be well predicted, suggesting that the unified hardening law that allows flexible plastic modulus variation with the stress state inside the bounding surface is suitable for describing the natural Boom Clay behavior. Moreover, the volume change behavior including the shear dilatancy is well described with the non-associated flow rule. By adopting different hardening parameters in the loading/unloading/reloading processes, the hysteresis loop behavior under full unloading-reloading cycles (with loading compression and extension) can also be well described.

5. Conclusion

A kinematic hardening model is developed for describing some important features of natural stiff clays under cyclic loadings. The model uses general expressions for the yield surface, the

MCC yield surface being a special case. A unified kinematic hardening law associated with the kinematic yield surface is introduced, enabling the plastic modulus to vary flexibly when the kinematic yield surface approaches the bounding surface. The kinematic surface can be in contact with the bounding surface but never intersect with it. The non-associated flow rule adopted allows the shear and volume change behavior to be satisfactorily described, especially the shear dilatancy behavior. In addition, by introducing three model parameters for describing the hardening rate in the first loading/unloading/reloading process, the cyclic loading behavior of natural stiff clays can be flexibly modeled. With the unified hardening law introduced, the constitutive equations of the model can be simply formulated based on the consistency condition for the kinematic yield surface. Therefore, the proposed kinematic hardening model can be easily implemented in a numerical code using a stress integration scheme as for the MCC model.

Comparisons between the model predictions and the experiment data from the tests on natural Boom Clay show that the model is capable to capture the overall stress-strain behavior along different loading paths under cyclic loading conditions. In particular, the model can satisfactorily describe the complex case of oedometer tests where the deviator stress can become negative during unloading.

Acknowledgements

The authors are grateful to the Chinese Scholar Council and the Euridice/Ondraf for their financial supports.

Reference:

[1] G. Baldi, T. Hueckel, A. Peano, R. Pellegrini, Developments in modelling of thermo-hydro-geomechanical behaviour of boom clay and clay-based buffer materials, Commission of the European Communities, Nuclear Science and Technology (1991) EUR 13365/1 and EUR 13365/2.

[2] Y. J. Cui, X. P. Nguyen, A. M. Tang, X. L. Li, An insight into the unloading/reloading loops on the compression curve of natural stiff clays, Applied Clay Science 83 (2013) 343–348.

[3] S. Horseman, M. Winter, D. Entwistle, Geotechnical characterization of boom clay in relation to the disposal of radioactive waste, Final report, EUR 10987. Luxembourg: Commission of the European Communities.

[4] X. P. Nguyen, Étude du comportement chimico-hydro-mécanique des argiles raides dans le contexte du stockage de déchets radioactifs, Ph.D. thesis, Université Paris-Est, France (2013).

[5] Y. Dafalias, L. Herrmann, A bounding surface soil plasticity model, in: International Symposium on Soils under Cyclic and Transient Loading, Swansea, UK, Vol. 1, 1980, pp. 335–345.

[6] Y. Dafalias, Bounding surface plasticity. i: Mathematical foundation and hypoplasticity, Journal of Engineering Mechanics 112 (9) (1986) 966–987.

[7] H. Hirai, An elastoplastic constitutive model for cyclic behaviour of sands, International journal for numerical and analytical methods in geomechanics 11 (5) (1987) 503–520.

[8] C. Aboim, W. Roth, Bounding surface plasticity theory applied to cyclic loading of sand, in: International Symposium on Numerical Models in Geomechanics, 1982, pp. 65–72.

[9] O. Zienkiewicz, Z. Mroz, Generalized plasticity formulation and applications to geomechanics, Mechanics of engineering materials (1984) 655–679.

[10] K. Hashiguchi, Z.-P. Chen, Elastoplastic constitutive equation of soils with the subloading surface and the rotational hardening, International Journal for Numerical and Analytical Methods in Geomechanics 22 (3) (1998) 197–227.

[11] Z. Mroz, On the description of anisotropic workhardening, Journal of the Mechanics and Physics of Solids 15 (3) (1967) 163–175.

[12] A. Al Tabbaa, D. M. Wood, An experimentally based bubble model for clay, in: Proceedings of the 3rd International Symposium on Numerical Models in Geomechanics (NUMOG III), Elsevier, 1989, pp. 90–99.

[13] S. Wheeler, A. Naatanen, M. Karstunen, M. Lojander, An anisotropic elastoplastic model for soft clays, Canadian Geotechnical Journal 40 (2) (2003) 403–418.

[14] Z. Mroz, V. Norris, O. Zienkiewicz, The application of an anisotropic hardening model in the analysis of elasto-plastic deformation of soils, Geotechnique 29 (1).

[15] G. Houlsby, A. Puzrin, Principles of hyperplasticity: an approach to plasticity theory based on thermodynamic principles, Springer, 2006.

[16] M. Zytynski, M. Randolph, R. Nova, C. Wroth, On modelling the unloading-reloading behaviour of soils, International Journal for Numerical and Analytical Methods in Geomechanics 2 (1) (1978) 87–93.

[17] S. J. van Eekelen, P. van den Berg, The delft egg model, a constitutive model for clay, in: DIANA Computational Mechanics '94, Springer, 1994, pp. 103–116.

[18] R. Borja, C. Lin, F. Montáns, Cam-clay plasticity, part iv: Implicit integration of anisotropic bounding surface model with nonlinear hyperelasticity and ellipsoidal loading function, Computer methods in applied mechanics and engineering 190 (26-27) (2001) 3293–3323.

[19] H. S. Yu, C. Khong, J. Wang, A unified plasticity model for cyclic behaviour of clay and sand, Mechanics Research Communications 34 (2) (2007) 97–114.

[20] C. Hu, H. Liu, W. Huang, Anisotropic bounding-surface plasticity model for the cyclic shakedown and degradation of saturated clay, Computers and Geotechnics 44 (2012) 34–47.

[21] A. F. L. Amorim, Thermo-hydro-mechanical behaviour of two deep belgium clay formations: Boom and ypresisan clay, Ph.D. thesis, Universitat Politècnica de Catalunya, Spain (2011).

[22] S. Horseman, M. Winter, D. Entwisle, Triaxial experiments on boom clay, Enginnering Geology Special Publication (1993) 35–35.

[23] F. Bernier, X. L. Li, W. Bastiaens, Twenty-five years' geotechnical observation and testing in the tertiary boom clay formation, Géotechnique 57 (2) (2007) 229–237.

[24] P. Delage, T. T. Le, A. M. Tang, Y. J. Cui, X. L. Li, Suction effects in deep boom clay block samples, Géotechnique 57 (1) (2007) 239–244.

[25] P. Y. Hong, Development and explicit integration of a thermo-mechanical model for saturated clays, Ph.D. thesis, Université Paris-Est, France (2013).

[26] T. Lê, Comportement thermo-hydro-mécanique de l'argile de boom, Ph.D. thesis, École Nationale des Ponts et Chaussées (2008).

[27] Y. F. Deng, A. M. Tang, Y. J. Cui, X. P. Nguyen, X. L. Li, L. Wouters, Laboratory hydro-mechanical characterisation of boom clay at essen and mol, Physics and Chemistry of the Earth, Parts A/B/C 36 (17) (2011) 1878–1890.